Ratiometric Fluorescence Imaging

International Edition: DOI: 10.1002/anie.201802972
German Edition: DOI: 10.1002/ange.201802972

Bioorthogonal Conjugation Directed by a Sugar-Sorting Pathway for Continual Tracking of Stressed Organelles

*Zhongwei Xue[+], Enkang Zhang[+], Jian Liu, Jiahuai Han, and Shoufa Han**

Dedicated to Professor Ronald E. Viola

Abstract: *Selective and continuous tracking of dynamic organelles is crucial for modern biology. We herein report a ship-in-a-bottle strategy for tagging lysosomes by a strain-promoted azide–alkyne cycloaddition to couple a pH sensor (RC) with mannose-6-carboxylate (M6C) actively transported into lysosomes through cell sorting. In contrast to classical acidotropic sensors, which are prone to dissipate from lysosomes, M6C-RC formed in situ is stably trapped in lysosomes without resort to lysosomal acidity and exhibits "always-on" blue fluorescence to pinpoint lysosomes and red-to-blue fluorescence ratios indicative of the lysosomal pH value. These advantages enable tracking of stressed lysosomes, and necrosis to be differentiated from apoptosis on the basis of lysosomal pH changes. The cell-sorting-mediated bioorthogonal tagging strategy offers a new route to track stressed organelles with disrupted physiological organelle–probe affinity.*

Fluorescence imaging aided by advancing labeling technologies provides unprecedented opportunities for spatiotemporal visualization of diverse biological processes in realms ranging from biomolecules to organelles and to whole organisms.[1] Cell fate is largely shaped by the combined activity of distinct subcellular organelles, which are often targeted with synthetic probes driven by organelle parameters, such as mitochondrial potential and lysosomal acidity.[2] Although widely used, these probes are prone to dissipate upon organelle stress, such as loss of lysosomal acidity. Lysosomes are acidic organelles essential to myriad cellular events, including immunity, cell homeostasis, and cell death.[3] Abnormal lysosomes are manifested in numerous pathological conditions.[4] For example, the lysosomal pH value is markedly elevated in lysosomal storage diseases,[5] whereas altered lysosome positioning occurs in cancer metastasis.[6] Therefore, approaches capable of continual tracking of stressed lysosomes would be useful to decipher the roles of lysosomes in biology and diseases.

Herein we report sugar-sorting-pathway-directed intra-organelle bioorthogonal conjugation (SPIBC) to tag lysosomes, whereby dibenzocyclooctyne (DBCO)-appended mannose-6-caboxylate (^{DBCO}M6C) is actively transported into lysosomes through an endogenous mannose-6-phosphate (M6P) sorting pathway, and then undergoes strain-promoted azide–alkyne cycloaddition with a diffusible azide-bearing rhodamine-lactam/coumarin dyad (^{Az}RC) to give M6C-RC in lysosomes (Figure 1). After its formation in situ, M6C-RC is maintained in lysosomes independent of lysosomal acidity and exhibits pH-relevant ratiometric fluorescence, which enables tracking of lysosome alterations in exocytosis and cell-death signaling events.

Lysosomes are routinely imaged with sensors that accumulate in lysosomes as driven by protonation.[2] However, these acidotropic sensors are prone to dissipate from lysosomes upon pH elevation. For example, a rhodamine-lactam-based pH sensor suffers from significant signal loss from stressed lysosomes in apoptosis.[7] In view of this limitation, we sought to trap diffusible optical sensors through bioorthogonal conjugation with an entity that could be maintained in lysosomes independent of lysosomal acidity. Ubiquitous in mammalian cells, M6P receptors mainly address newly biosynthesized hydrolases with M6P-terminating glycans to lysosomes.[8] M6P is degradable by phosphatases. As the structural analogue of M6P, M6C possesses a lateral carboxylate group bridged by a methylene linker and is immune to phosphatase hydrolysis.[9] To hijack the M6P sorting pathway, M6C was used as the lysosome-localizing entity to conjugate pH-reporting ^{Az}RC in lysosomes (Figure 1).[10]

We hence prepared ^{DBCO}M6C and ^{Az}RC, which readily combined in vitro to give M6C-RC as a mixture of two regioisomers, as evidenced by HPLC and mass spectrometry analysis (see Figures S1 and S2 in the Supporting Information). pH titration showed that M6C-RC and RC both displayed "always-on" blue coumarin fluorescence (CM), which moderately declined as the pH value decreased, and acidity-mediated "turn-on" rhodamine-X fluorescence (ROX), which intensified as the pH value decreased

[*] Z. Xue,[+] E. Zhang,[+] Dr. J. Liu, Prof. S. Han
State Key Laboratory for Physical Chemistry of Solid Surfaces
Department of Chemical Biology, College of Chemistry and Chemical Engineering, Key Laboratory for Chemical Biology of Fujian Province
MOE Key Laboratory of Spectrochemical Analysis and Instrumentation, and Innovation Center for Cell Signaling Network, Xiamen University, Xiamen, 361005 (China)
E-mail: shoufa@xmu.edu.cn
Prof. J. Han
State Key Laboratory of Cellular Stress Biology, Innovation Center for Cell Signaling Network, School of Life Sciences, Xiamen University
Xiamen, 361005 (China)
[+] These authors contributed equally.

Supporting information, including experimental procedures, confocal microscopy analysis of cell staining with M6C-RC, effects of temperature and M6P on SPIBC, PI/annexin V staining, western blotting, and a cell cytotoxicity assay, and the ORCID identification number(s) for the author(s) of this article can be found under: https://doi.org/10.1002/anie.201802972.

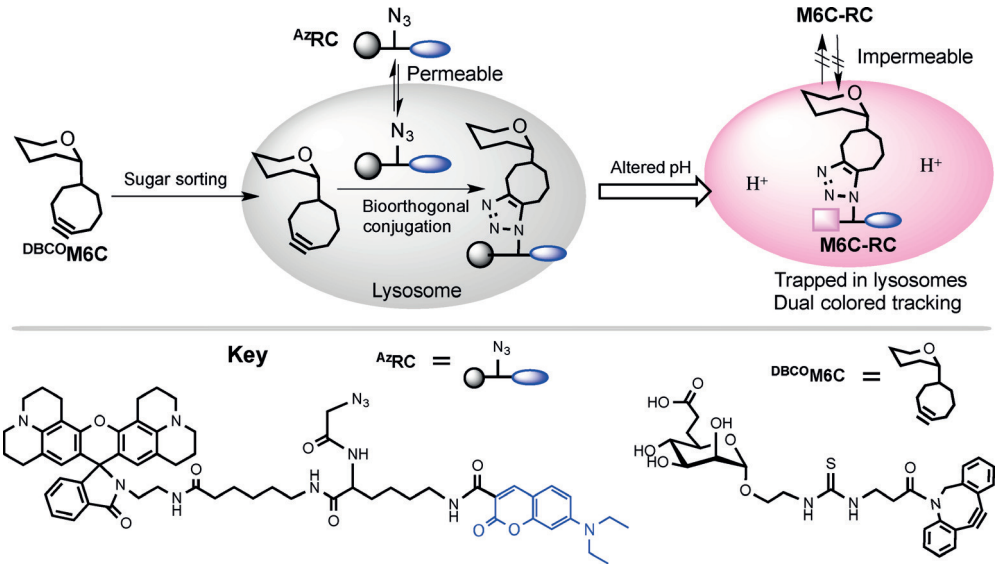

Figure 1. Lysosome imaging by sugar-sorting-pathway-directed intralysosomal bioorthogonal conjugation (SPIBC). Delivered into lysosomes by M6P sorting, ^{DBCO}M6C reacts with ^{Az}RC through azide–alkyne cycloaddition to give M6C-RC, which is stably trapped in lysosomes and shows pH-relevant ratiometric fluorescence. The key shows the chemical structures of ^{DBCO}M6C and ^{Az}RC.

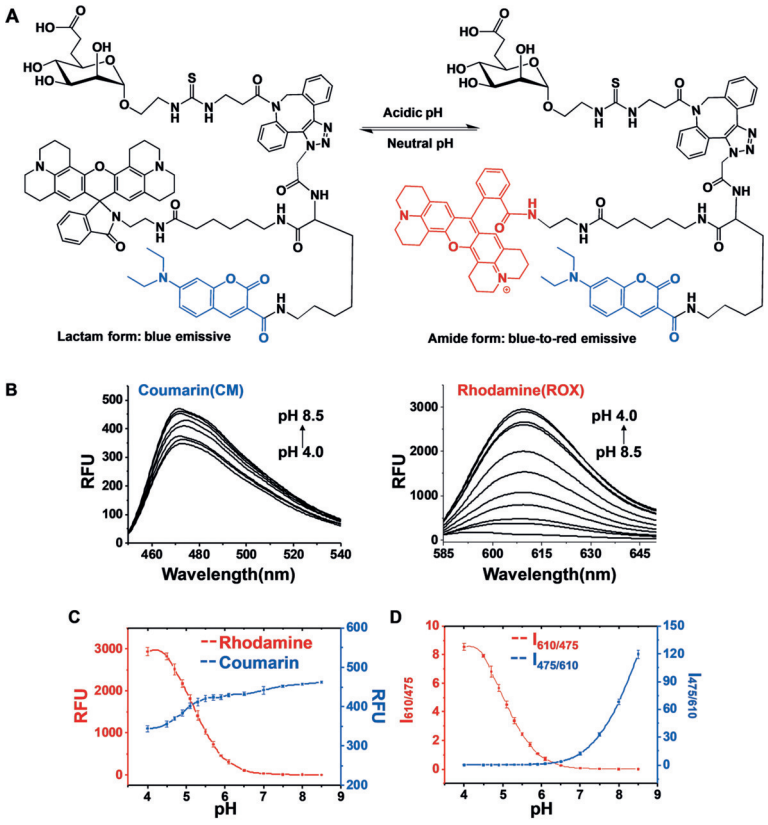

Figure 2. pH-mediated ratiometric fluorescence of M6C-RC. A) Proton-triggered isomerization of M6C-RC gives "turn-on" ROX fluorescence. B) CM and ROX fluorescence of M6C-RC (5 μM) at pH 4.5–8.5 (λ_{ex}: 435 nm for CM, 590 nm for ROX). C) pH titration curves of M6C-RC; fluorescence emission of ROX (λ_{em}: 605 nm) and CM (λ_{em}: 475 nm) plotted against the pH value. D) pH-dependent fluorescence ratios of ROX (I_{610}) to CM (I_{475}).

(pH 6.5–4.5; Figure 2; see also Figure S3), owing to proton-mediated fluorogenic isomerization of the rhodamine lactam (Figure 2 A).[7,11] Ratiometric imaging affords enhanced accuracy relative to single-intensity fluorescence imaging.[12] The sensitive blue-to-red fluorescence ratios of M6C-RC at pH 6.0–4.5 are beneficial for monitoring subtle changes in lysosomal acidity (Figure 2 D).

To ascertain SPIBC-mediated targeting of lysosomes, HeLa cells expressing GFP-Lamp2 (green-fluorescent-protein-fused lysosome-associated membrane protein 2) were cultivated with ^{DBCO}M6C/^{Az}RC. Confocal microscopy analysis revealed bright and punctate ROX and CM signals, which eclipsed GFP-Lamp2 in cells stained with ^{DBCO}M6C/^{Az}RC (Figure 3 A). As GFP-Lamp2 is a protein marker specific for lysosomes, colocalization of CM/ROX signals with GFP-Lamp2 proves stringent selectivity of SPIBC for lysosome imaging. Relative to M6C-RC synthesized in vitro, staining with ^{DBCO}M6C/^{Az}RC exhibited much brighter lysosomal fluorescence and was kinetically favored (see Figure S4), thus verifying that ^{DBCO}M6C is preferentially delivered into lysosomes over M6C-RC by cells. Furthermore, lysosomes were effectively illuminated with ^{DBCO}M6C/^{Az}RC in a variety of cell lines, including A549, L929, and MCF-7 cells (see Figure S5), thus proving the applicability of SPIBC for effective lysosome imaging in diverse cell lines.

To assess lysosomal retention of M6C-RC formed in situ, we treated GFP-Lamp2$^+$ HeLa cells with ^{DBCO}M6C/^{Az}RC in the presence of baflomycin A1, which is a potent inhibitor of V-ATPase and neutralizes lysosomes. The observed loss of ROX signals in cells treated with baflomycin A1 is in line with acidity-mediated ROX fluorescence (Figure 4). By contrast, discrete CM signals remained intense and colocalized with GFP-Lamp2 in cells (Figure 4; see also Figure S6), thus proving that the retention of M6C-RC in lysosomes is independent of lysosomal acidity. Relative to hydrophilic ^{Az}RC, M6C-RC generated in situ is rather hydrophilic, which could hinder diffusion across the lysosomal mem-

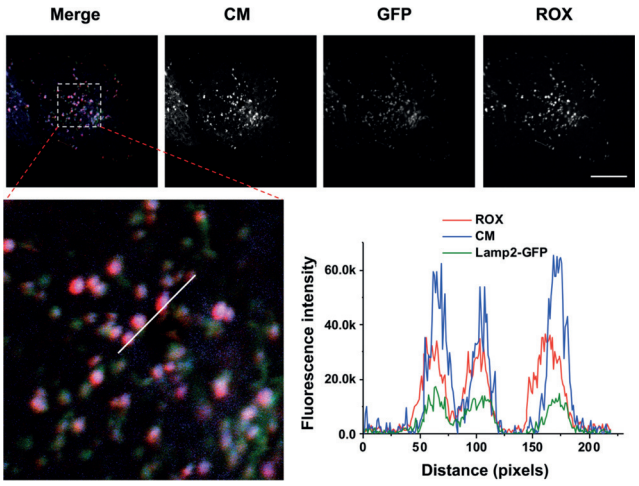

Figure 3. SPIBC-mediated selective imaging of lysosomes. GFP-Lamp2^{+} HeLa cells stained with ^{DBCO}M6C/^{Az}RC were probed by confocal microscopy. Plots of the fluorescence of CM, ROX, and GFP were measured along the line shown in the zoomed image and revealed the colocalization of CM/ROX signals with Lamp2-GFP. Scale bar, 10 μm.

brane and thus contribute to acidity-independent retention of M6C-RC in lysosomes (Figure 1).

We next probed the structural factors required for SPIBC. ^{Az}RC is prone to protonation of the spirolactam to give the amide form (see Figure S3), which enables acidity-dependent lysosomal staining. As expected, HeLa cells treated with ^{Az}RC alone displayed loss of lysosome-associated fluorescence upon treatment with baflomycin A1 (Figure 4), a phenomenon characteristic of acidotropic sensors owing to dissipation from neutralized lysosomes, thus highlighting the essential role of ^{DBCO}M6C in SPIBC. Relative to ^{DBCO}M6C, ^{amino}M6C is devoid of the DBCO moiety, whereas DBCO-conjugated mannose (^{DBCO}M) lacks the lateral carboxylate group. Loss of ^{Az}RC from lysosomes as triggered by baflomycin A1 was also observed in cells costained with ^{amino}M6C or ^{DMCO}M (Figure 4), which validates the crucial roles of the DBCO moiety and carboxylate group of ^{DBCO}M6C in SPIBC. Likewise, in cells cultivated with ^{DBCO}M6C and azide-free RC, ROX/CM fluorescence vanished upon lysosomal neutralization mediated by baflomycin A1 (see Figure S7), thus verifying the dependence of the azido moiety of ^{Az}RC for SPIBC-mediated acidity-independent imaging.

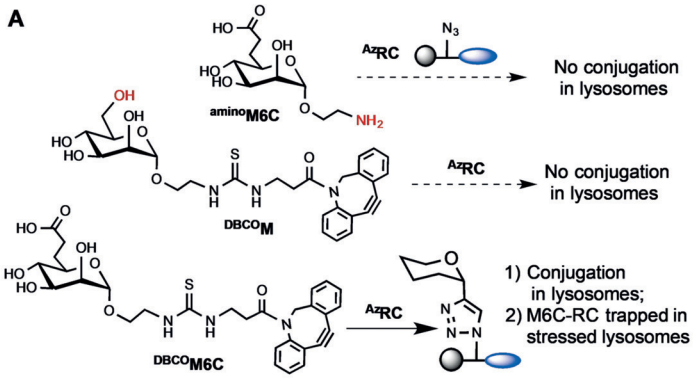

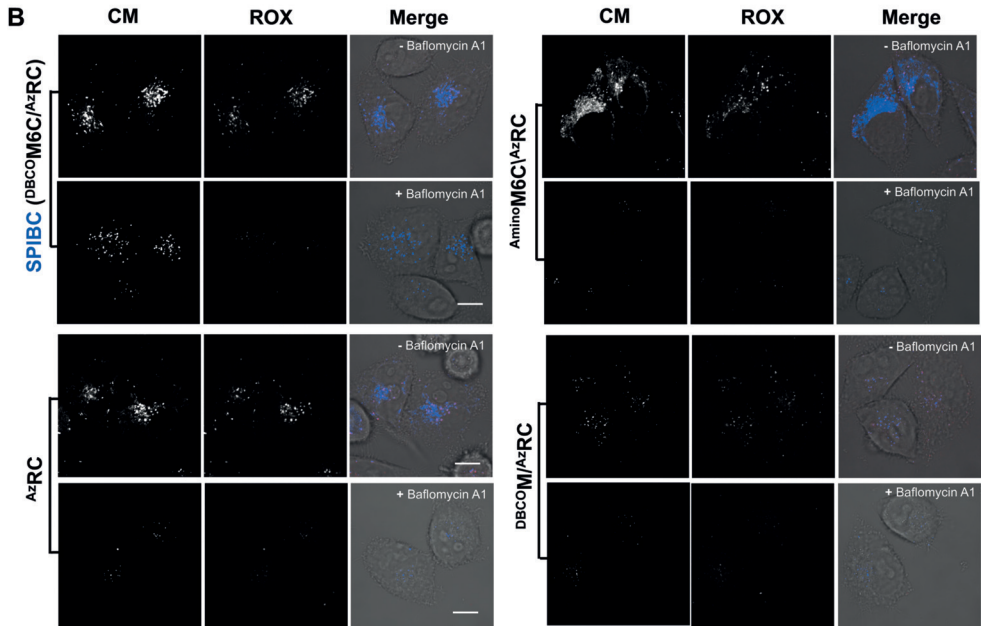

Figure 4. Acidity-independent lysosomal imaging by SPIBC. A) Chemical structures of ^{amino}M6C and ^{DBCO}M as compared to ^{DBCO}M6C. B) Confocal microscopic images of ^{Az}RC-treated HeLa cells cultured with ^{DBCO}M6C, ^{Amino}M6C, ^{DBCO}M, or no sugar derivative, in the presence or absence of baflomycin A1. Scale bars, 10 μm.

GFP-Lamp2$^+$ HeLa cells were treated with chloroquine to induce lysosomal membrane permeabilization.[13] SPIBC analysis revealed decreased colocalization of CM with GFP (see Figure S8), indicative of leakage of M6C-RC from permeabilized lysosomes, thus showing that membrane integrity is required for SPIBC-based imaging. These results establish that the azido group of ^{Az}RC, and M6C/DBCO domains of ^{DBCO}M6C, are prerequisites for SPIBC. SPIBC was significantly inhibited at 4 °C relative to 37 °C (see Figure S9), thus supporting the involvement of membrane trafficking in the transport of ^{DBCO}M6C into lysosomes by membrane-anchored M6P receptor. Furthermore, we observed dose-dependent inhibition of SPIBC by exogenous M6P (see Figure S10), the natural ligand of M6P receptor. The competition between M6P and ^{DBCO}M6C validates the involvement of M6P sorting in SPIBC. Given the liability of acidotropic dyes to leak from neutralized lysosomes, acidity-independent SPIBC-based imaging offers unprecedented opportunities to track cellular events featuring lysosomal pH elevation.

Lysosomal exocytosis underlies a number of critical cellular functions, such as plasma membrane repair, transmitter release, and immune degranulation.[14] Exocytosis is elusive to imaging owing to the loss of acidotropic dyes from exocytosing lysosomes. Therefore, distinct approaches have been developed to image exocytosis.[15] Shown to stain lysosomes without resort to lysosomal acidity, SPIBC was evaluated for its efficacy in imaging exocytosis. RBL-2H3 cells loaded with ^{DBCO}M6C/^{Az}RC were stimulated with ionomycin, a calcium ionophore capable of stimulating lysosome exocytosis.[16] We observed that lysosomes exhibited punctate CM signals and diminished ROX fluorescence in the vicinity of the cell surface in ionomycin$^+$ cells (see Figure S11). The loss of ROX signals is consistent with the previous observation of lysosomal pH elevation upon exocytosis,[17] and the bright CM fluorescence showed retention of in situ conjugated M6C-RC in lysosomes during exocytosis. The capability of SPIBC to track exocytosing lysosomes proves its utility for the spatiotemporal visualization of dynamic lysosomes with an altered lysosomal pH value and positioning in live cells.

Deregulated cell death is a common feature of several diseases, such as cancers. Cell death occurs through a number of distinct routes,[18] whereby lysosomes participate in distinct cell-death pathways.[3a,19] Apoptosis is considered cell-autonomous and non-inflammatory, whereas necrosis often leads to

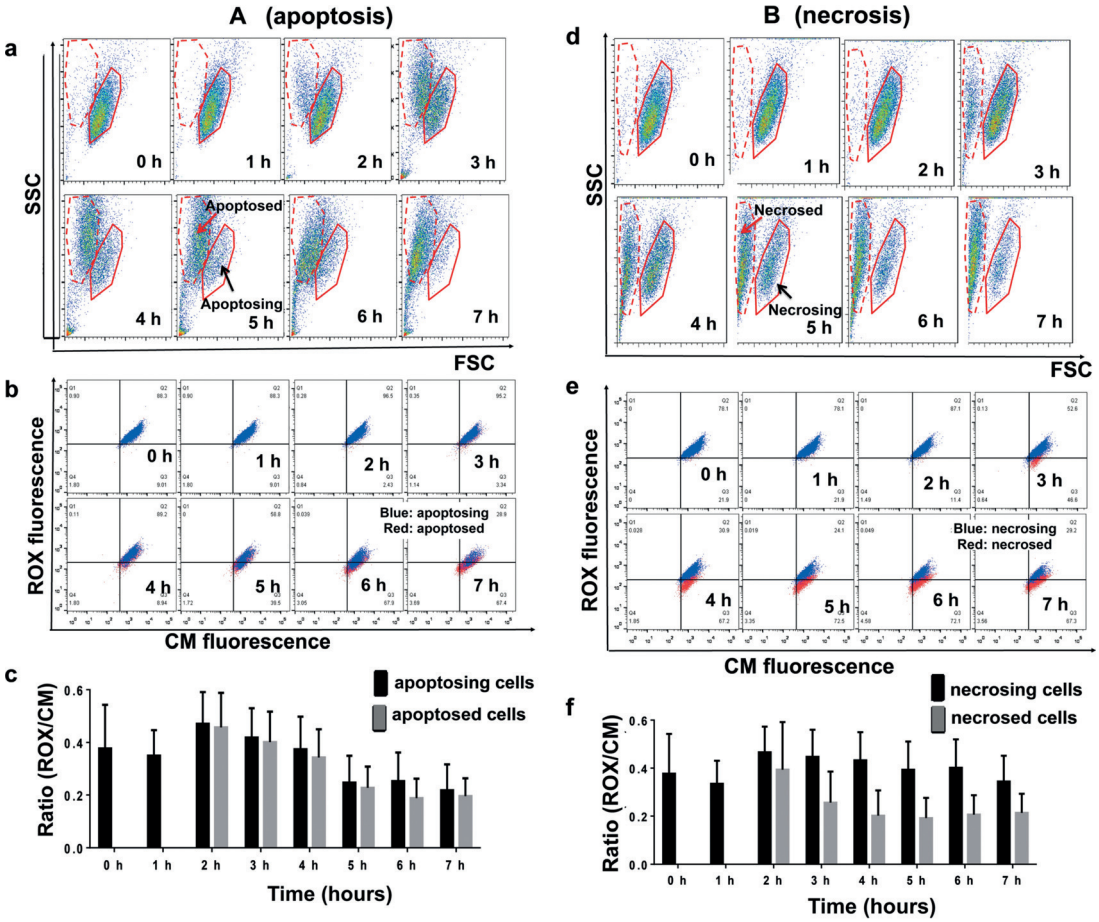

Figure 5. Distinct lysosomal pH-alteration profiles in apoptosis and necroptosis as revealed by SPIBC. RIP$_3^+$ HeLa cells prestained with ^{DBCO}M6C/^{Az}RC were cultivated with A) TNF/Smac or B) TNF/Smac/Z-VAD and then monitored over time by flow cytometry. Cell populations in CM versus ROX dot plots (b, e) were gated identically to those in bivariate dot plots of FSC versus SSC (a, d). Statistical results of ROX/CM ratios were measured by flow cytometry (c and f). Error bars represent the standard deviation of 10000 cells.

inflammation.[20] We then applied SPIBC to image lysosomal responses in cell death using RIP3$^+$ (receptor-interacting protein 3) HeLa cells treated with Smac and human tumor necrosis factor-a (TNF) to trigger apoptosis, or with Smac/TNF/Z-VAD to trigger necroptosis, a programmed form of necrosis.[21] Time–course analysis by bivariate dot plots of forward scatter (FSC) versus side scatter (SSC) clearly revealed the formation of two new cell populations (Figure 5a,d) owing to apoptosis and necrosis, as confirmed by western blotting analysis and staining with annexin V/propidium iodide (see Figures S12 and S13). The dot plots of ROX versus CM, indicative of the lysosomal pH value, show that apoptosed cells displayed attenuated ROX/CM ratios of similar magnitudes to those of apoptosing cells, whereas necrosed cells featured substantially decreased ROX/CM ratios relative to necrosing cells (Figure 5b,e). Furthermore, confocal microscopy confirmed clearly declined ROX fluorescence and ROX/CM ratios in necrosed cells relative to necrosing cells (Figure 6). Apart from the common tendency to lose lysosomal acidity in both cell-death modalities, these results show that lysosomal pH elevation is greater in necrosed cells than necrosing cells, but remained alike in apoptosed cells and apoptosing cells, thus demonstrating the utility of SPIBC to discern lysosome changes in closely related cell-death subtypes.

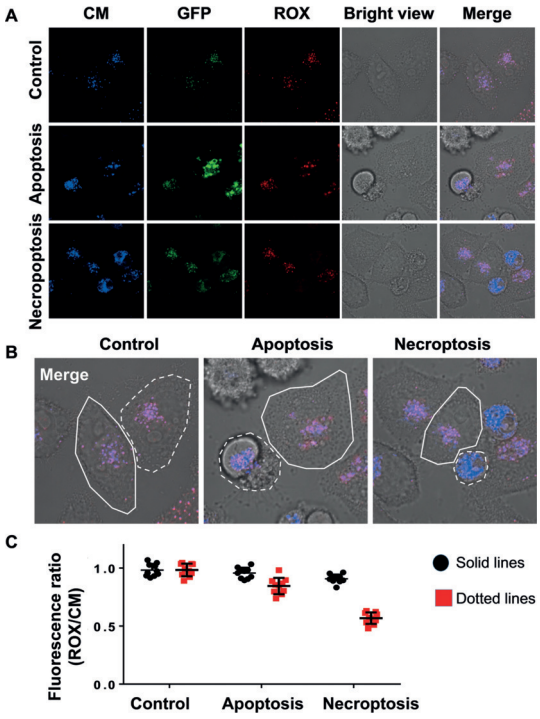

Figure 6. Discerning lysosomal pH changes in apoptosis versus necroptosis with SPIBC. A) RIP_3^+/Lamp2-GFP$^+$ HeLa cells loaded with ^{DBCO}M6C/^{Az}RC were further cultivated with TNF/Smac or TNF/Smac/Z-VAD before confocal microscopy analysis. B) Apoptosed cells and necrosed cells are circled with a dotted line in the zoomed images. Apoptosing cells and necrosing cells are indicated by solid lines. C) Statistical results of ROX/CM ratios were measured by confocal microscopy. Error bars represent the standard deviation of 10 representative cells. Scale bars, 10 μm.

Metabolic bioorthogonal labeling in biological systems enables visualization of various biomolecules, including glycans, nucleic acids, and lipids.[22] In the context of these advances, we have shown the use of sugar-sorting-pathway-mediated intralysosomal bioorthogonal conjugation for imaging of stressed lysosomes, which represents a further extension of bioorthogonal chemistry in bioimaging.

In conclusion, we have demonstrated a ship-in-a-bottle strategy to track stressed lysosomes using sugar-sorting-pathway-directed bioorthogonal conjugation. Actively transported into lysosomes through cellular M6P sorting, ^{DBCO}M6C undergoes strain-promoted azide–alkyne cycloaddition with ^{Az}RC in lysosomes. In situ formed M6C-RC, stably maintained in lysosomes without resort to lysosomal acidity, enables spatiotemporal tracking of stressed lysosomes, and necroptosis to be discerned from apoptosis on the basis of lysosomal pH changes. Manifested in myriad diseases, stressed organelles are often challenging to track with classical organelle sensors owing to frequent loss of physiological organelle–probe affinity. Apart from visualizing stressed lysosomes, SPIBC holds potential to be adapted to other specific organelles with the aid of cognate organelle-destined trafficking or sorting pathways, thus representing a new perspective from which to probe organelle stress in biology and diseases.

Acknowledgements

This research was supported by grants from NSF China (21775130, 21572189, 21602185) and the Fundamental Research Funds for the Central Universities (20720160052, 20720150047), Xiamen University. J.H. was supported by grants from NSF China (91429301, 31420103910, 31330047, 31221065) and the National Scientific and Technological Major Project (2013ZX10002-002).

Conflict of interest

The authors declare no conflict of interest.

Keywords: apoptosis · bioorthogonal reactions · cell death · ratiometric fluorescence imaging · stressed organelles

How to cite: *Angew. Chem. Int. Ed.* **2018**, *57*, 10096–10101
Angew. Chem. **2018**, *130*, 10253–10258

[1] a) F. Leblond, S. C. Davis, P. A. Valdes, B. W. Pogue, *J. Photochem. Photobiol. B* **2010**, *98*, 77–94; b) K. M. Dean, A. E. Palmer, *Nat. Chem. Biol.* **2014**, *10*, 512–523; c) S. H. Shim, C. Xia, G. Zhong, H. P. Babcock, J. C. Vaughan, B. Huang, X. Wang, C. Xu, G. Q. Bi, X. Zhuang, *Proc. Natl. Acad. Sci. USA* **2012**, *109*, 13978–13983; d) E. M. Sevick-Muraca, *Annu. Rev. Med.* **2012**, *63*, 217–231.
[2] C. de Duve, T. de Barsy, B. Poole, A. Trouet, P. Tulkens, F. Van Hoof, *Biochem. Pharmacol.* **1974**, *23*, 2495–2531.
[3] a) G. Kroemer, M. Jaattela, *Nat. Rev. Cancer* **2005**, *5*, 886–897; b) P. Saftig, J. Klumperman, *Nat. Rev. Mol. Cell Biol.* **2009**, *10*, 623–635.

[4] C. Settembre, A. Fraldi, D. L. Medina, A. Ballabio, *Nat. Rev. Mol. Cell Biol.* **2013**, *14*, 283 – 296.
[5] A. Kogot-Levin, M. Zeigler, A. Ornoy, G. Bach, *Pediatr. Res.* **2009**, *65*, 686 – 690.
[6] N. Fehrenbacher, M. Jaattela, *Cancer Res.* **2005**, *65*, 2993 – 2995.
[7] Z. Xue, H. Zhao, J. Liu, J. Han, S. Han, *ACS Sens.* **2017**, *2*, 436 – 442.
[8] a) P. Ghosh, N. M. Dahms, S. Kornfeld, *Nat. Rev. Mol. Cell Biol.* **2003**, *4*, 202 – 212; b) M. Gary-Bobo, P. Nirde, A. Jeanjean, A. Morere, M. Garcia, *Curr. Med. Chem.* **2007**, *14*, 2945 – 2953.
[9] a) A. Jeanjean, M. Garcia, A. Leydet, J. L. Montero, A. Morere, *Bioorg. Med. Chem.* **2006**, *14*, 3575 – 3582; b) O. Vaillant, K. El Cheikh, D. Warther, D. Brevet, M. Maynadier, E. Bouffard, F. Salgues, A. Jeanjean, P. Puche, C. Mazerolles, P. Maillard, O. Mongin, M. Blanchard-Desce, L. Raehm, X. Rebillard, J. O. Durand, M. Gary-Bobo, A. Morere, M. Garcia, *Angew. Chem. Int. Ed.* **2015**, *54*, 5952 – 5956; *Angew. Chem.* **2015**, *127*, 6050 – 6054.
[10] a) N. J. Agard, J. A. Prescher, C. R. Bertozzi, *J. Am. Chem. Soc.* **2004**, *126*, 15046 – 15047; b) J. C. Jewett, C. R. Bertozzi, *Chem. Soc. Rev.* **2010**, *39*, 1272 – 1279.
[11] a) W. Zhang, B. Tang, X. Liu, Y. Liu, K. Xu, J. Ma, L. Tong, G. Yang, *Analyst* **2009**, *134*, 367 – 371; b) T. Hasegawa, Y. Kondo, Y. Koizumi, T. Sugiyama, A. Takeda, S. Ito, F. Hamada, *Bioorg. Med. Chem.* **2009**, *17*, 6015 – 6019; c) X. Wu, M. Yu, B. Lin, J. Han, S. Han, *Chem. Sci.* **2015**, *6*, 798 – 803; d) M. Yu, X. Wu, B. Lin, J. Han, L. Yang, S. Han, *Anal. Chem.* **2015**, *87*, 6688 – 6695; e) Z. Xue, H. Zhao, J. Liu, J. Han, S. Han, *Chem. Sci.* **2017**, *8*, 1915 – 1921.
[12] a) Q. Wang, L. Zhou, L. Qiu, D. Lu, Y. Wu, X. B. Zhang, *Analyst* **2015**, *140*, 5563 – 5569; b) X. Z. Zhang, T. Zhang, S. Shen, J. Miao, B. Zhao, *J. Mater. Chem. B* **2015**, *3*, 3260 – 3266; c) G. Li, D. Zhu, L. Xue, H. Jiang, *Org. Lett.* **2013**, *15*, 5020 – 5023; d) B. Dong, X. Song, C. Wang, X. Kong, Y. Tang, W. Lin, *Anal. Chem.* **2016**, *88*, 4085 – 4091; e) Z. Li, S. Wu, J. Han, L. Yang, S. Han, *Talanta* **2013**, *114*, 254 – 260; f) G. J. Song, S. Y. Bai, J. Luo, X. Q. Cao, B. X. Zhao, *J. Fluoresc.* **2016**, *26*, 2079 – 2086.
[13] K. R. Schultz, A. L. Gilman, *Leuk. Lymphoma* **1997**, *24*, 201 – 210.
[14] E. D. Gundelfinger, M. M. Kessels, B. Qualmann, *Nat. Rev. Mol. Cell Biol.* **2003**, *4*, 127 – 139.
[15] a) D. Asanuma, Y. Takaoka, S. Namiki, K. Takikawa, M. Kamiya, T. Nagano, Y. Urano, K. Hirose, *Angew. Chem. Int. Ed.* **2014**, *53*, 6085 – 6089; *Angew. Chem.* **2014**, *126*, 6199 – 6203; b) D. Zenisek, J. A. Steyer, W. Almers, *Nature* **2000**, *406*, 849 – 854; c) G. Miesenböck, D. A. De Angelis, J. E. Rothman, *Nature* **1998**, *394*, 192 – 195; d) D. Liu, J. A. Martina, X. S. Wu, J. A. Hammer 3rd, E. O. Long, *Immunol. Cell Biol.* **2011**, *89*, 728 – 738.
[16] A. Rodríguez, P. Webster, J. Ortego, N. W. Andrews, *J. Cell Biol.* **1997**, *137*, 93 – 104.
[17] H. Xu, D. Ren, *Annu. Rev. Physiol.* **2015**, *77*, 57 – 80.
[18] a) G. Kroemer, L. Galluzzi, P. Vandenabeele, J. Abrams, E. S. Alnemri, E. H. Baehrecke, M. V. Blagosklonny, W. S. El-Deiry, P. Golstein, D. R. Green, M. Hengartner, R. A. Knight, S. Kumar, S. A. Lipton, W. Malorni, G. Nunez, M. E. Peter, J. Tschopp, J. Yuan, M. Piacentini, B. Zhivotovsky, G. Melino, *Cell Death Differ.* **2009**, *16*, 3 – 11; b) S. J. Dixon, K. M. Lemberg, M. R. Lamprecht, R. Skouta, E. M. Zaitsev, C. E. Gleason, D. N. Patel, A. J. Bauer, A. M. Cantley, W. S. Yang, B. Morrison, B. R. Stockwell, *Cell* **2012**, *149*, 1060 – 1072; c) M. Overholtzer, A. A. Mailleux, G. Mouneimne, G. Normand, S. J. Schnitt, R. W. King, E. S. Cibas, J. S. Brugge, *Cell* **2007**, *131*, 966 – 979.
[19] S. Aits, M. Jaattela, *J. Cell Sci.* **2013**, *126*, 1905 – 1912.
[20] T. Vanden Berghe, A. Linkermann, S. Jouan-Lanhouet, H. Walczak, P. Vandenabeele, *Nat. Rev. Mol. Cell Biol.* **2014**, *15*, 135 – 147.
[21] S. He, L. Wang, L. Miao, T. Wang, F. Du, L. Zhao, X. Wang, *Cell* **2009**, *137*, 1100 – 1111.
[22] a) C. Y. Jao, M. Roth, R. Welti, A. Salic, *Proc. Natl. Acad. Sci. USA* **2009**, *106*, 15332 – 15337; b) C. Y. Jao, A. Salic, *Proc. Natl. Acad. Sci. USA* **2008**, *105*, 15779 – 15784; c) J. T. Ngo, D. A. Tirrell, *Acc. Chem. Res.* **2011**, *44*, 677 – 685.

Manuscript received: March 11, 2018
Accepted manuscript online: June 11, 2018
Version of record online: July 4, 2018

